Journal of Opt. Society of America A, 24(3):618-625, 2007.

Multiscale complex moments of the local power spectrum

Stefan Karlsson and Josef Bigun

School of Information Science,

Halmstad University, P.O. Box 823,

*SE-301 18 Halmstad, Sweden**

Complex moments of the local power spectrum (CMP) are investigated in a multiscale context. The multiscale CMPs are shown to approximate well the 1D angular fourier transform of the band in question. This observation is used to derive further properties of the power spectrum in terms of texture orientations or n-folded symmetry patterns. A method is presented to approximate the power spectrum using only separable filtering in the spatial domain. Interesting implications to the Gabor decomposition are shown. The number of orientations in the filter bank is related to the order of n-folded symmetry detectable. Furthermore, the multiscale CMPs can be estimated incrementally in the spatial domain which is both fast and reliable. Experiments on power spectrum estimation, orientation estimation and texture segmentation are presented.

OCIS codes: 100.2960, 100.5010, 100.5760

*Electronic address: s.karlsson@phys.uu.nl, josef.bigun@ide.hh.se

1. Introduction

Frequency based features are an important set of texture descriptors[1,2,3]. A common approach is the use of a bank of Gabor filters to estimate the local spectrum[4]. After being extracted, the *Gabor spectrum* (the coarse description of the spectrum given by the ordered Gabor filter responses of the neighborhood, e.g. as seen in figure 1) can be put to a scheme for deriving new features. This paper is concerned with the *complex moments of the local power spectrum* (*CMPs*). These descriptors have been shown to have simple interpretations in the spatial domain, in terms of local orientation and n-folded symmetry[5].

We study here the CMP descriptors when they are calculated on distinct frequency bands, i.e. in multiscale. Under this multiscale assumption we uncover novel properties of the CMPs. These include that multiscale CMPs are DFT coefficients of the power spectrum. Further more, we show that the discriminative power of CMPs can be increased in multiscale without increasing their order.

This paper *is not* stating that the CMPs are superior to Gabor filters in descriptive power. Indeed, our message is that CMPs and Gabor magnitudes are very similar to the degree that in multiscale, they describe the same quantity, although in different domains. CMPs are beneficial in how the information is encoded and can be efficiently computed.

The Gabor spectrum is a coarser version of the local spectrum (low-pass filtered and sampled). In particular, sampling schemes where the sampling is finer closer to the zero frequency are often used, an approach which is motivated from findings in both image statistical studies as well as neurological research[6].

A practical outcome of our findings is that the number of jointly detectable directions is determined by the number of orientations in the Gabor filter bank. This provides simple visual interpretations in terms of n-folded symmetries in the spatial domain. Conversely, when using too few Gabor filters the information loss is equivalent to losing the ability to detect jointly existing orientations in the image.

A consequence of the conclusions is that the multiscale CMPs can be calculated completely in the spatial domain (without the use of Gabor filters) by creating the frequency bands via a laplacian pyramid. Complex moments estimated this way are compared to the Gabor filters in the tasks of unsupervised texture segmentation, orientation estimation and power spectrum estimation. The multiscale CMPs describe the frequency band uniquely up to a 1D fourier transform which makes it possible to estimate the power spectrum without

the use of Gabor filters.

In section 2 we outline the underlying concepts of local spectrum analysis, Gabor filters and directionality estimation by CMPs. The precise definition of multiscale CMPs is given in section 3 where we also present several of their properties. In section 4 a method for estimating the CMPs in the spatial domain is presented, which also leads to a scheme for estimating the power spectrum. We compare the two descriptors (Gabor power spectrum vs the spatially estimated multiscale CMPs) in section 5. We present the results from experiments in unsupervised texture segmentation. Finally, section 6 concludes the paper.

2. Local Spectrum Analysis

The *local spectrum* $F_{\vec{x}_0}(\vec{\omega})$ is defined as

$$F_{\vec{x}_0}(\vec{\omega}) = \mathcal{F}\left\{f(\vec{x}_0 - \vec{x})w_\sigma(\vec{x})\right\} = \iint f(\vec{x}_0 - \vec{x})w_\sigma(\vec{x}) \exp\left(-j\vec{\omega}^T\vec{x}\right) dx \tag{1}$$

where $\mathcal{F}$ is the Fourier transform, $j = \sqrt{-1}$ and $w_\sigma(\vec{x})$ is the window function with width parameter σ. The local spectrum is thus arrived at by considering the neighborhood about a pixel as an individual image, and taking its Fourier transform. This is a valuable tool to image analysis[1,2,3].

The global spectrum of an image is obtained when the window is large, i.e. when $\sigma \to \infty$ in Eq 1. We will omit *local* and/or *global* and refer only to the spectrum when it is obvious from the context or when the theory applies to both. Our concept of multiscale is to process the information found in separate bands (annuli) of the spectrum, centered around the dc component. We will use the terms *scale* and *frequency band* interchangeably. The magnitude squared of the local spectrum is defined as the *local power spectrum* $\rho(\vec{\omega}) = |F_{\vec{x}_0}(\vec{\omega})|^2$.

We note that Eq 1 can be viewed as a convolution, if $\vec{x}_0$ is the new spatial variable and $\vec{\omega}$ is assumed fixed. This corresponds to applying a Gabor filter[4] $w_\sigma(\vec{x}) \exp\left(-j\vec{\omega}^T\vec{x}\right)$ on the image which yields samples of the local spectrum at a given position $\vec{x}_0$.

Different flavors of Gabor filters can be constructed by placing 2D low pass filters in the spectrum e.g. as seen in figure 1 (not frequency responses of low pass filters, but the actual placement of low pass filters in the Fourier domain). We will henceforth use the *log-Gabor functions*[7,8,9] which are gaussian low pass filters in logarithmic polar coordinates($log(z)$) of the spectrum (which captures human frequency sensitivity better than cartesian frequency coordinates). Using polar coordinates (still in the frequency domain) these filters are given by

$$\Psi_{r_o\phi_o}(r,\phi) = \exp\left(-\frac{(\log(\frac{r}{r_o}))^2}{2(\log(\frac{\sigma_r}{r_o}))^2}\right)\exp\left(-\frac{(\phi-\phi_o)^2}{2\sigma_\phi^2}\right) \quad (2)$$

where r_o and ϕ_o are the placements of the filter in the radial and angular variable and σ_r and σ_ϕ are the widths of the filter radially and angularly, *in the Fourier domain.*

The Gabor filter responses are samples of a coarse local spectrum. The *Gabor spectrum* is the ordered set of all responses, at some point of interest $\vec{x}_0$, which corresponds to a low pass filtered and sampled local spectrum, as seen in figure 1.

A. n-Folded Symmetry

An image consisting of only parallel lines is said to have one orientation. If two sets of mutually parallel lines exists but with different directions, it is said to have two orientations.

To generalize this we now define n-folded symmetry[5]. An image is said to have n-folded symmetry(n even, positive integer) if it has $p = \frac{n}{2}$ orientations such that the angle between each successive orientation is constant. Then, a 2-folded symmetry image is one that has a single orientation. A 4-folded symmetry image has only 2 orientations that are orthogonal, etc. It is worth noting that the symmetry is defined with respect to the orientations in the image, not the intensity (gray values) of the image. There is essential difference to the concept of *Rotational symmetry of order n*, where the entire image is invariant to rotations of $\frac{2\pi}{n}$. For n-folded symmetry, the joint directions of high energy are invariant to rotations of $\frac{2\pi}{n}$, but the texture itself is not necessarily so. Figure 2 shows an example of a texture with perfect 6-folded symmetry (it does however lack Rotational symmetry).

For each orientation of a texture, there exists nonzero values concentrated to a line through the origin of the power spectrum. To find the amount and direction of n-folded symmetry in an image, one could therefore search for best matching line structures in the power spectrum.

The *Structure Tensor*[10], maps the 2-folded case onto a well known problem from rigid body mechanics solved by the inertia tensor. This idea has been extended by ways of *complex moments* to find the group orientation pattern for the n-folded case[5]. Complex moments were introduced to spatial shape analysis as a technique to derive moment descriptors invariant to rotation[11,12]. The complex moments of a function $f(x,y)$ are defined by

$$I_{a,b}\{f\} = \iint (x+jy)^a (x-jy)^b f(x,y)dxdy \quad (3)$$

Where a and b are non-negative integers. It is known that these moments, when taken on the power spectrum, have crisp n-folded symmetry interpretations[13]. Here the notation $I_{p,p}$ and $I_{2p,0}$ will only apply to moments taken on the power spectrum (CMPs) defined as

$$I_{2p,0} = \iint (u+jv)^{2p}\rho(u,v)dudv \;=\; (\lambda_p^{max} - \lambda_p^{min})\exp(j2\varphi_p^{min}) \tag{4}$$

$$I_{p,p} = \iint |u+jv|^{2p}\rho(u,v)dudv \;=\; \lambda_p^{max} + \lambda_p^{min} \tag{5}$$

where λ_p^{max}, λ_p^{min} and φ_p^{min} are for the n-folded structures ($n = 2p$), respectively, measure of worst fit, best fit and the group direction of the best fit[5]. The $I_{p,p}$ and $|I_{2p,0}|$ measures are by construction rotationally invariant, while $\angle I_{2p,0}$ contains only rotational information. The function ρ is the power spectrum, $\rho(u,v) = |F(u,v)|^2$. An alternative to Eq. (4) and Eq. (5) can be found by use of the Parseval-Plancherel relationship yielding a method based directly in the spatial domain:

$$I_{2p,0} \;=\; \iint ((D_x + jD_y)^p f)^2 d\vec{x} \tag{6}$$

$$I_{p,p} \;=\; \iint |(D_x + jD_y)^p f|^2 d\vec{x} \tag{7}$$

For example, $I_{4,0} = \iint (f_{xx} - f_{yy} + 2jf_{xy})^2 dxdy$, where f_{xy} denotes second order partial derivatives w.r.t. x and y.

3. Multiscale CMPs

We will continue to use ρ to denote the power spectrum, but will for convenience write $\rho(u,v)$ when using cartesian frequency coordinates and $\rho(r,\phi)$ for polar frequency coordinates. We will adopt the notation $\left[\mathcal{F}\left\{h(\phi)\right\}\big|_{(p)}\right]$, to mean the 1 dimensional Fourier transform of the 2π periodic function $h(\phi)$ evaluated at $\omega = p \in \mathbb{Z}$.

The *single-scale CMPs* are defined as the complete set of CMPs for all p but where the image is bandlimited to a band (annulus) at radius R, i.e. the power spectrum has nonzero values essentially only on a narrow circular band located R units from the origin. By taking sufficiently distinct and dense single-scale CMPs we obtain the *multiscale CMPs*. We will use the notation $I_{2p,0}^{(R)}$ to denote that it is a CMP over the band represented by R.

Given an arbitrary image with power spectrum $\rho(r,\phi)$, we can limit it to a narrow band at R by a band-pass filtering:

$$\rho_R(r,\phi) = \rho(r,\phi)g(r-R,\sigma) \tag{8}$$

where $g(r,\sigma)$ is the Gaussian function with standard deviation σ.

With a power spectrum of the form in Eq. 8, the formula for complex moments becomes:

$$\begin{aligned} I_{2p,0}^{(R)} &= \iint (u+jv)^{2p} \rho_R(u,v) du dv = \\ &= \iint r^{2p+1} \rho_R(r,\phi) \exp\left(j\phi 2p\right) dr d\phi \end{aligned} \tag{9}$$

We are interested in the case when the frequency bands are narrow; i.e. when σ of the gaussian in Eq. (8) is small. We take the limit of the gaussian which will then act as a Dirac delta, i.e. when $\sigma \to 0$ Eq. (9) reduces to:

$$I_{2p,0}^{(R)} = C_p \left[\mathcal{F}^{-1} \left\{ \rho(R,\phi) \right\} \big|_{(2p)} \right] \tag{10}$$

where $C_p = R^{2p+1}\sqrt{2\pi}$ and the transform is taken over the variable ϕ. In the same way we have that, for the limit $\sigma \to 0$

$$I_{p,p}^{(R)} = C_p \left[\mathcal{F}^{-1} \left\{ \rho(R,\phi) \right\} \big|_{(0)} \right] \tag{11}$$

The sequence of single-scale CMPs for $p \in \mathbb{Z}^+$ encodes discrete samples of the 1 dimensional Fourier transform of $\rho(R,\phi)$. Furthermore, these CMPs contain ***all*** the information of the transform. This can be seen by inspecting the $\rho(R,\phi)$ function. Formally $\rho(R,\phi) = |F(R,\phi)|^2$ and due to hermitian symmetry $|F(R,\phi)| = |F(R,\phi+\pi)|$, i.e. $\rho(R,\phi)$ is a periodic function with period π. The Fourier transform of a function with period π is a discrete function with the sampling interval of two units. Inspecting Eq. (10) and (11) we see that the interval between two samples are indeed two, and we can say that the entire transform is contained in the CMPs. The CMPs are in effect the coefficients of a Fourier series expansion of $\rho(R,\phi)$.

We denote with $\xi(p)$:

$$\xi(p) = \left[\mathcal{F}^{-1} \left\{ \rho(R,\phi) \right\} \big|_{(2p)} \right] = \lim_{\sigma \to 0} \frac{I_{2p,0}^{(R)}}{C_p}$$

We now consider only one band of the Gabor spectrum that covers the circle with radius R. We will denote the Gabor sampled function as $\rho(R, k\frac{\pi}{q})$ $(k \in \mathbb{Z})$ while remembering that it is low pass filtered as well as sampled. The coefficients $\xi(p)$ will be periodic with period q and are the discrete fourier transform (DFT) of $\rho(R, k\frac{\pi}{q})$:

$$\xi(p) = \sum_{k=0}^{q-1} \rho(R, k\frac{\pi}{q}) \exp\left(\frac{jk\pi 2p}{q}\right) = \lim_{\sigma \to 0} \frac{I_{2p,0}^{(R)}}{C_p} \tag{12}$$

If the amount of low pass that is performed by the Gabor filters is sufficient for the down-sampling then no aliasing effects will be present, otherwise $\xi(p)$ will be distorted and the estimated symmetries of order $n = 2p$ will be unreliable. This shows the importance of having Gabor filters that are wide enough in the angular direction. On the other hand, if the Gabor filters are too wide then the low pass filtering will be too intense resulting in the values of $\xi(p)$ for higher p (above some threshold p_{max}) to vanish and thereby their descriptive power to diminish.

We have now reached the point where we can show the following theorem:

Theorem 1 *If energy is concentrated only to a thin band of the global spectrum (thus also for all the local spectra assuming appropriate window size), and local neighborhoods are described by Gabor filter responses with q different orientations, then the maximum n-folded symmetry that can be estimated in any local neighborhood is* $n_{max} = q - 1 - mod(q + 1, 2)$.

All orders, $n \leq n_{max}$, are possible to estimate whereas $n > n_{max}$ are impossible to estimate. n_{max} could be expressed as $q - 1$, with the understanding that n_{max} must be an even number.

A. Proof of Theorem 1

We will work with $p = \frac{n}{2}$. The estimates of n-folded symmetry is performed by the CMPs according to Eq. 4 and 5. The relation between the Gabor filter responses and the CMPs are given by a 1D discrete Fourier transform (Eq. 12).

The sampling frequency of the function $\rho(R, k\frac{\pi}{q})$ is $\frac{q}{\pi}$ and the frequency components are the CMPs (Eq. 12). The Nyquist-Shannon sampling theorem states that the sampling frequency must be strictly greater than twice the highest frequency component, i.e.

$$2p < q \quad \Leftrightarrow \quad p \leq \frac{q-1}{2} \quad \Leftrightarrow \quad p_{max} = \left\lfloor \frac{q-1}{2} \right\rfloor$$

$$n_{max} = 2p_{max} = q - 1 - mod(q + 1, 2)$$

End of proof

To estimate 2-folded symmetry ($n = 2$, i.e. regular orientation estimation) in a neighborhood a minimum of three filter orientations ($q = 3$) are required of the filter bank. For 4-folded (2 simultaneous orientations), 5 filter orientations are needed and so on.

As the Gabor decomposition is made coarser higher order symmetries are removed from the individual bands but not from the entire image. This has practical consequences which we illustrate by the example of figure 2. The texture of figure 2 contains three orientations (perfect six folded symmetry) when the full spectrum is considered. However when isolating the relevant narrow bands as can be done by Eq. (8) and illustrated in figure 2, only one orientation will result. The points of high energy are situated in different bands whereas no band contains more than one direction.

Given that enough bands are partitioned, the texture of figure 2 requires thus only three filter orientations. In multiscale, the texture contains only 2-folded symmetry, whereas the entire image contains 6-folded symmetry. In the power spectrum of figure 2, we can gather a maximum of six energy points (corresponding to totally n=6) in a single band when making the bands wider. In general, it is clear that individual bands *may contain lower order symmetries* than that of the whole image. However, it is also evident that individual bands *may* ***never*** *contain higher order symmetries* than that of the whole image. Figure 2 shows that when bands are considered together (not separately as in Theorem (1)) then fewer filter orientations may be possible. For a reliable estimate, where any band may contain the symmetry of the whole image, Theorem (1) provides the minimum number of filter orientations.

4. Spatial Implementation and Power Spectrum Estimation

Our assumption for multiscale is that energy is concentrated to only narrow bands in the spectrum. This can be done by Gabor decomposition of the texture and then considering the bands of the Gabor spectrum by themselves. Another approach can be taken by implementing a multiscale decomposition, e.g. using Mexican hat filters or separable gaussian filters (both essentially a laplacian pyramid).

After the laplacian pyramid has been built the CMPs can be approximated by the spatial operations of Eq. (6) and (7) which in turn are very fast to estimate using separable filtering. Regardless of what filtering scheme chosen to construct the pyramid this spatial domain method is faster, compared to extracting the full Gabor spectrum and applying Eq. (4) and (5). Besides speed, another major benefit is that we bypass the angular partitioning of the Gabor decomposition all together. Because the isotropic bands are intact in the pyramid, we can extract any order of multiscale CMP on the levels of the pyramid, *incrementally*. That

is, after estimating up to pth order CMP, if the $(p+1)$th order CMP is required, then the old filtering results are still used. However, for the Gabor filters, if a filter bank of q orientations has been applied and the need for $q+1$ orientations arises, then a new filter bank must be constructed and the response of the old one discarded. For example, in estimating the power spectrum, it is in general not known how many orientations are needed or equivalently, how many orders of CMPs are required. With both CMPs and Gabor filters, one could formulate a measure of energy that could be used as an indicator of whether enough descriptors have been extracted. However, with Gabor filters it would be required to iteratively extracting a full decomposition, and then discarding it if the demand was not met.

When the bands are narrow the properties of Eq. (10) and (11) will hold and the Gabor power spectrum and the multiscale CMPs converge to achieve the same goal, namely to represent the band. However, they describe the band uniquely in different domains that are Fourier transforms of each other. From this observation, we can formulate a scheme of estimating the power spectrum directly from the multiscale CMPs:

1. For each level of a laplacian pyramid, apply the Eq. (6) and (7) to generate a sequence of different order CMPs, $I_{1,1}$ and $I_{2p,0}$ for $p \in [1, N]$. Form the sequence $\xi(p) = \left\{ \frac{I^*_{N,0}}{C_N}; \ldots; \frac{I^*_{2,0}}{C_1}; \frac{I_{1,1}}{C_1}; \frac{I_{2,0}}{C_1}; \ldots; \frac{I_{2N,0}}{C_N} \right\}$ (* is complex conj.) for $p \in [-N, N]$.

2. A low pass and sampled version of the power spectrum band is given by $\rho(R, k\frac{\pi}{q}) = \mathcal{F}\{\xi(p)\}$. The number of samples is $q = 2N + 1$ (compare Theorem (1))

5. Experimental Results

We present experimental results on texture segmentation, power spectrum estimation and orientation estimation. The common goal with all three experiments is to show the descriptive power of CMPs calculated in the spatial domain and compare CMPs with the Gabor filter magnitudes.

A. Texture Segmentation

We present here the results of experiments on segmenting real textures with clear boundaries where the classification is performed unsupervised. This segmentation is ***not*** performed in a rotationally invariant manner, although the rotation can be easily factored out as outlined in section 2 A, yielding truly rotation invariant features. We choose not to do so here, as this would make the comparison with the unprocessed Gabor filters unreasonable. We

experiment on the three images of figure 3, which have been used by several studies on texture analysis[14,15,16]) allowing comparison. All three images are constructed by using 7 different textures positioned as patches in 16 different, equal sized areas. The patches have been placed so as to maximize the combinations of borders and the textures have been normalized to unit mean and variance. The textures of left and center images have been taken from difficult real world aerial photographs and the right figure uses the textures from the Brodatz database. All images are gray scale with 8 bit color depth (256 shades) and are 256 by 256 pixels in size.

We compared the multiscale CMPs with the Gabor power spectrum (used directly as features) to show that they are closely related as seen in Eq. (4) and (5) (we expect the results to be comparable between the two methods). To make the comparison on an equal basis, care was taken in the construction of the Laplacian pyramid so that the same radial partitioning was performed for both approaches.

The CMPs were calculated in the spatial domain, on the levels of the laplacian pyramid. For the Gabor filter, the Log-Gabor scheme of Eq. (2) was used.

For all the results presented, we used an experimental setup of five levels of the pyramid, with the corresponding radial partitioning for the Gabor filters. We varied the orders of the CMPs that were extracted from each level. As features we selected the real and imaginary parts of the CMPs. The largest of feature vectors corresponded to $p \in \{1, 2\}$. The features were extracted from each level of the pyramid independently, resulting in a total of 25 features for $p \in \{1, 2\}$ and 15 features for $p = 1$. For the Gabor filters, we varied the number of filters that partition in the angular direction of each band. We used 3 and 5 directions for two experiments, resulting in exactly the same amount of features as for the CMPs.

We reduced the dimensionality by Principal Component Analysis[17] (PCA). For the Segmentation, where each pixel was assigned a class label, an efficient boundary estimation algorithm[18] was implemented (which is related to an older approach[19] based on a quadtree decomposition). The algorithm requires an independent clustering technique at a low resolution of the features. We used the fuzzy c-means clustering algorithm[20].

Figures 4 and 5 display the results of segmentation using the CMPs and Gabor filter magnitudes respectively(the results for p3 are near perfect and thus omitted). Table 1 shows the percentage of correct pixels classified. As the number of features increase, the segmentation improves for both methods. For both set of features, the class boundaries become

more accurate, and classes are less likely to merge. Interestingly, CMPs perform noticeably better on all 3 images, with the arguable exception p3 which is strongly homogenous and is segmented quite easily by both approaches.

Inspecting p3 we notice that most of the textures contain higher order symmetry (only two textures contain one dominant orientation, in the upper right corner and lower left corner of the image). We know from Eq. (4) and (5) that the CMPs $I_{1,1}$ and $I_{2,0}$ contain the amount and orientation of linear symmetry. How is it possible that these measures are able to discriminate between *all* of the textures of the rightmost image when no such symmetry exist in most of them? Similarly, we know from Theorem (1) that using fewer orientations in the Gabor decomposition is equivalent to excluding higher orders of symmetries from the bands, so how come the second experiment was successful for only 3 orientations in the filter bank (which leaves only second order symmetry contents in the bands)? The answer is given by the example in figure 2 from which we know that textures exist with higher order symmetries globally, but with lower orders in the individual bands. The textures of the rightmost image, while containing higher order symmetries viewed from the global scale, have only second order contents in some of the partitioned bands. This result thus speaks in favor of lower order symmetry descriptors combined with multiscale in applications. In practice, the need for excessively high order CMPs can be circumvented by a finer radial partitioning resulting in more levels for the pyramid, as figure 2 illustrates.

Also for the left and center images we note that the segmentation is performed quite well using features corresponding to $p = 1$ which is partly accredited to the phenomenon of figure 2 and partly due to first order symmetry truly being present.

There are 3 major reasons for the results being different between the CMPs and Gabor decomposition. Firstly, the widths of the bands are not infinitesimal. Although the same radial partitioning is used, only when the bands are infinitesimally narrow will the two methods be identical. Secondly, the filters for performing angular low-pass within the bands differ between the methods. Thirdly, both encode the same information, yet one format may be better suited for texture segmentation(direct versus fourier representation).

B. Orientation Estimation

Figure 6 shows a frequency modulated test (FM-test) image. The direction of the wave changes angularly and the frequency depends on the radius (measured from the center). The FM-test image will be used for comparing orientation estimated in two different ways:

a) from the Gabor spectra, and ***b)*** the spatial approach outlined in section 4.

A single frequency band in the spectrum will be equivalent to a band also in the spatial domain of the FM-test image. We will study $\angle I_{2,0}$ encoding the first order direction angle, on one such band. To use the Gabor power spectrum to estimate $\angle I_{2,0}$, we apply Eq. 12, which directly relates the square magnitudes of the Gabor responses to $I_{2,0}$. For these experiments we chose the parameter of the Gabor filters to be $\sigma_\phi = \frac{\pi}{2q}$.

Figure 7 shows the result of this experiment. The x-axis of figure 7 indicates a position in the ring of figure 6. The correct direction is given by the dotted line and the estimated by the full line. We note that the spatial method yields better estimate than the Gabor spectrum approach, as no oscillatory behavior is present in the right figure. This phenomenon is due to the angular sampling of the Gabor spectrum. For the spatial method, while we still partition bands radially in spectrum, no angular sampling is performed. The oscillatory behavior is due to the non-ideal low-pass filtering by the Gabor filters; the spatially estimated CMPs do not suffer from this drawback.

C. Power Spectrum Estimation

The approach outlined in section 4 was implemented. A band pass filter first partition one narrow band of the spectrum, corresponding to $\sigma = \frac{1}{40}$ and $R = \frac{\pi}{2}$ of Eq. (8) (the frequency domain is limited to $[-\pi, \pi]$). CMPs for orders up to and including $p = 11$ are extracted on the band pass filtered image (corresponding to one level of a laplacian pyramid) and used to estimate the power spectrum band along 21 sample points.

For the Gabor filters, the frequency band partitioning is selected to be similar to the band-pass described above. 21 filter orientations are present on the single band in the filter bank. The Gabor filtering is done completely in the Fourier domain. To estimate the power spectrum, the response of each filter is taken square magnitude and averaged, yielding 21 sample points describing the power spectrum along the band.

We used the left image of figure 3, which was also used for the texture segmentation experiment. The results are shown in figure 8, where we see that the CMPs and the Gabor filters describe approximately the same band. The difference in representation is mainly due the difference in the low pass performed. While the Gabor filters are Gaussian in the angular direction, the CMPs perform a brick-wall filtering in the frequency domain (this due to the finite number of CMPs used). We can make the CMPs converge better to the Gabor filters by dampening the higher order ones, but doing so will undermine the clear

orientation interpretation of Eq. (4).

6. Summary and Conclusions

We have shown that multiscale CMPs have useful properties for applications. By investigating the CMPs in a multiscale context, we have found them to ***i)*** approximate the 1D fourier transform of the band in question and ***ii)*** that the sequence of $I_{2p,0}$ together with $I_{1,1}$ uniquely determines the entire band. The $< I_{2p,0}$ determines the rotation of the band, and should therefore be omitted for applications where rotational invariance is desirable.

The multiscale CMPs can be calculated solely in the spatial domain, if a laplacian pyramid is constructed first, partitioning the spectrum into narrow bands. This in turn leads us to an alternative way of estimating the power spectrum, by using the CMPs without any Gabor filters. Being the Fourier transform of the Gabor power spectrum, CMPs are the frequency components of the band. By omitting some CMPs, we achieve low pass filtering in the angular direction.

These observations have enabled a novel interpretation of the Gabor Decomposition, in terms of orientation information. A relationship between the number of orientations in the Gabor filter bank and *reliable* orientation estimation (Theorem (1)) has been found.

We have shown experimental results that support the theory into power spectrum estimation, orientation estimation and texture segmentation. The results provide evidence of the multiscale CMPs strong descriptive power.

The low pass filtering of the Gabor filters make the orientation estimation less reliable, prone to oscillatory behavior. We showed that the spatial method is fast and accurate due to it leaving the bands intact when partitioning the spectrum. Furthermore, with CMPs the detail can be increased incrementally in contrast to the Gabor decomposition, where the results of previous coarser filter banks can not be used when the need for more orientations in the filter bank arise.

While the CMPs have many attractive properties, compared to using Gabor filters directly (especially in texture segmentation) it is in place to stress that the Gabor filter responses contain the phase information and not only the power spectrum. The CMPs do not have this capability because, by construction, they model the power spectrum. For applications where the phase matters, Gabor decomposition is still needed.

7. Acknowledgements

We thank Radhakrishnan Poomari and acknowledge his contribution to the texture segmentation[21], and also thank Werner Pomwenger for his helpful test images[22].

References

1. A.C Bovik, M. Clark, and W.S. Geisler, "Multichannel texture analysis using localized spatial filters", *IEEE PAMI*, vol. 12 pp. 55-73, 1990.
2. I. Fogel and D. Sagi, "Gabor filters as texture discriminator", *Biological Cybern.*, vol. 61, pp. 103-113, 1989.
3. A.K. Jain and F. Farrokhnia, "Unsupervised texture segmentation using Gabor filters", *Pattern Recognition*, vol. 24, pp 1167-1186, 1991.
4. D. Gabor, "Theory of communication", *Journal of the IEE*, vol. 93, pp. 429-457, 1946.
5. J. Bigun and J. M. H. du Buf, "N-folded Symmetries by Complex Moments in Gabor Space and Their Application to Unsupervised Texture Segmenation", *IEEE PAMI*, vol. 16, No.1, pp.80-87, January 1994.
6. R. B. H. Tootell and M. S. Silverman and E. Switkes and R. L. de Valois, "Deoxyglucose analysis of retinotopic organization in primate striate cortex",journal: *Science* vol 218, pp. 902-904, 1982
7. J. Bigun and J. M. H. du Buf, "N-folded Symmetries by Complex Moments in Gabor Space and Their Application to Unsupervised Texture Segmenation", *IEEE PAMI*, vol. 16, No.1, pp.80-87, January 1994.
8. D. Field. "Relation between the statistics of natural images and the response properties of cortical cells". *Journal of Optical Society of America A*, vol. 4, pp 2379-2394, 1987.
9. H. Knutsson, "Filtering and reconstruction in image processing", ph.d thesis: Linköping University, 1982.
10. J.Bigun and G. H. Granlund, "Optimal orientation detection of linear symmetry", *First Int. Conf. on Computer Vision*, London, June 1987, pp 433-438. *IEEE Comp. Soc. Press.*
11. S.S. Reddi. "Radial and Angular invariants for image identification". *IEEE Transactions on Pattern Analysis and Machine Intelligence*, vol. 3, pp 240-242, 1981.
12. Ming-Kuei Hu, "Visual Pattern Recognition by Moment Invariants", *IRE Transactions on Information Theory*, February 1962.

13. J. Bigun and T. Bigun and K. Nilsson, "Recognition by symmetry derivatives and the generalized structure tensor", *PAMI*, pp 1590-1605, vol 26, 2004.
14. J.M.H. du Buf, "Abstract processes in texture discrimination", *Spatial Vision* 6, pp. 221-242, 1992
15. G. Cristobal and J. Hormigo, "Texture segmentation through eigen-analysis of the Pseudo-Wigner distribution". *Pattern Recognition Letters* 20, pp. 337-345. 1999
16. D.A. Clausi and Huang Deng, "Design-based texture feature fusion using Gabor filters and co-occurrence probabilities", *IEEE Trans. on Im. Proc.* 14, pp. 925 - 936, 2005
17. R. Duda and P. Hart "Pattern classification and scene analysis", J. Willey, New York, 1973
18. P. Schroeter and J. Bigun, "Hierarchical image segmentation by multi-dimensional clustering and orientation-adaptive boundary refinement", journal:*Pattern Recognition*, vol. 28, no. 5, pp. 695–709, 1995.
19. M. Spann and R. Wilson, 'A quad-tree approach to image segmentation which combines statistical and spatial information", *Pattern Recognition*, vol. 18, pp. 257-269. 1985.
20. J.C. Bezdek, "Pattern recognition with fuzzy objective function algorithm", *Plenum Press*, New York, 1981.
21. S. Karlsson and R. Poomari, "Unsupervised Texture Segmentation using Multi-scale Complex moments", Master Thesis: *HALMSTAD UNIVERSITY, School of Information Science Computer and Electrical Engineering*, 2005.
22. W. Pomwenger, "Texture Classification by High Order Symmetry Derivatives of Gaussians", Master Thesis: *HALMSTAD UNIVERSITY, School of Information Science Computer and Electrical Engineering*, May 2003.

Table 1. Segmentation performance in percentage correctly classified pixels.

CMP features				Gabor features			
Config.	p1	p2	p3	Config.	p1	p2	p3
15 feats.	70	78	98	15 feats.	65	60	98
25 feats.	94	90	98	25 feats.	80	81	98

List of Figure Captions

Fig. 1. Example of rosette like partitioning of Gabor filters in the Fourier Domain. Center of Graph is the DC component. The position and relative scope of the filters are illustrated by the ellipses.

Fig. 2. Example of texture with 6-folded symmetry. ***a)*** texture in spatial domain, ***b)*** power spectrum, black indicates high energy, ***c)*** Same spectrum magnified with one circular band explicitly illustrated within gray, dashed lines (as partitioned e.g. by Eq. 8). showLinearGood.eps

Fig. 3. The test images used in the experiments.

Fig.4. segmentation results for multiscale CMPs, top row: $p = 1$, bottom row: $p \in \{1, 2\}$.

Fig. 5. segmentation results for Gabor power spectrum, top row: 3 orientations, bottom row: 5 orientations.

Fig. 6. Left, a frequency modulated test image, the axes of which are marked with fractions of π representing the spatial frequency. Right, the same image, but band pass filtered corresponding to one level of a laplacian pyramid. Note that only one circular band remains of the original.

Fig. 7. The graphs represent the estimated $(\arg(I_{2,0}^{(R)}))$ (full lines) as well as the accurate direction angle(dotted lines) on a ring in the FM-test image. Left, estimated with Gabor spectrum of 6 orientations, right estimated by spatial approach.

Fig. 8. The estimated power spectrum along one narrow band using Gabor filters (dotted) and CMPs (full line). Image used to estimate is the "p1" image of figure 3.

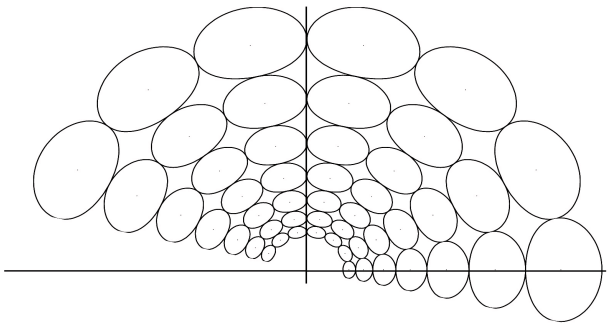

Fig. 1. Example of rosette like partitioning of Gabor filters in the Fourier Domain. Center of Graph is the DC component. The position and relative scope of the filters are illustrated by the ellipses. GaborExample.eps

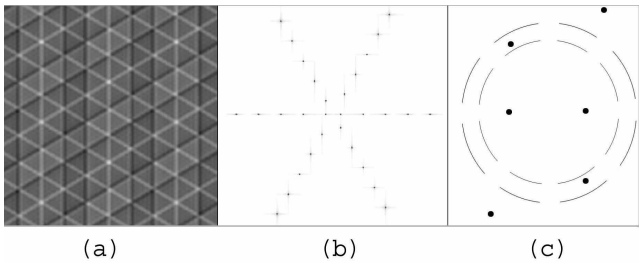

Fig. 2. Example of texture with 6-folded symmetry. ***a)*** texture in spatial domain, ***b)*** power spectrum, black indicates high energy, ***c)*** Same spectrum magnified with one circular band explicitly illustrated within gray, dashed lines (as partitioned e.g. by Eq. 8). showLinear-Good.eps

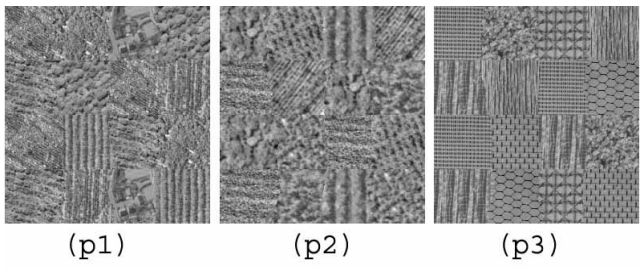

Fig. 3. The test images used in the experiments. px.eps

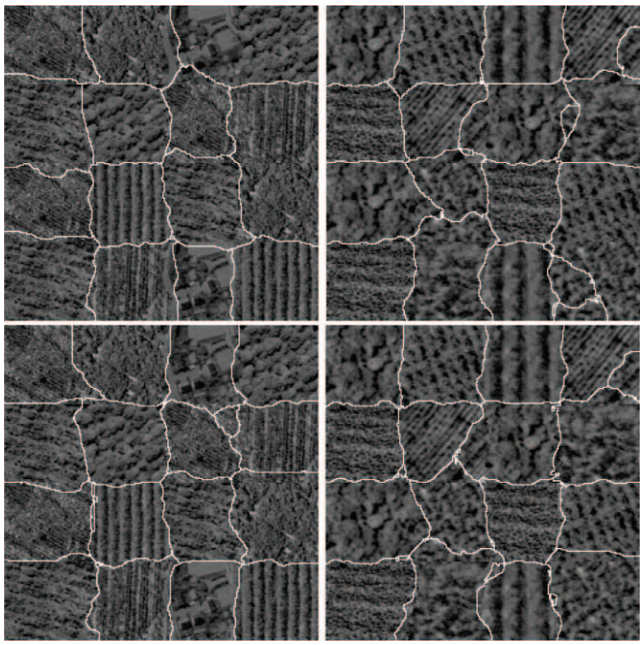

Fig. 4. segmentation results for multiscale CMPs, top row: $p = 1$ (15 features), bottom row: $p \in \{1, 2\}$ (25 features). finalRes.eps

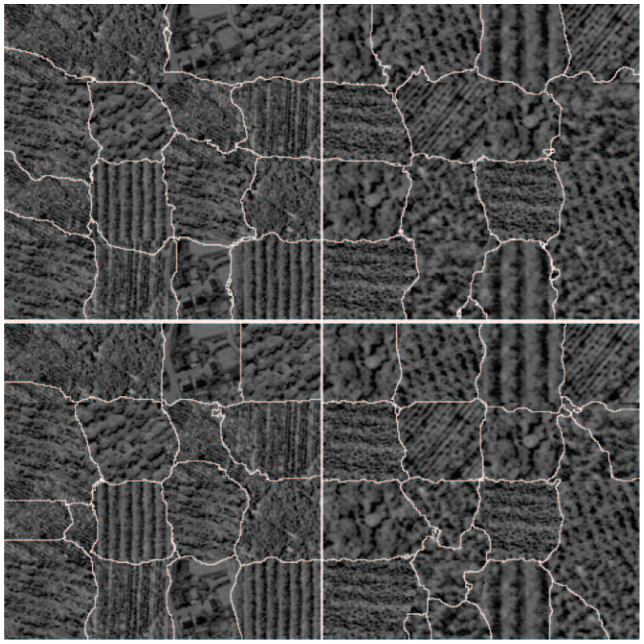

Fig. 5. segmentation results for Gabor power spectrum, top row: 3 orientations (15 features), bottom row: 5 orientations (25 features). finalGab.eps

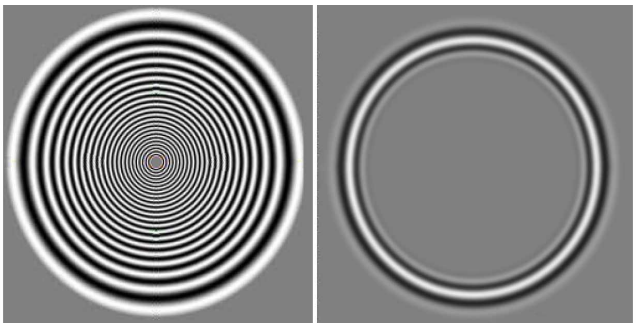

Fig. 6. Left, a frequency modulated test image, the frequency is decreasing with distance from center. Right, the same image, but band pass filtered corresponding to one level of a laplacian pyramid. Note that only one circular band remains of the original. fmtest.eps

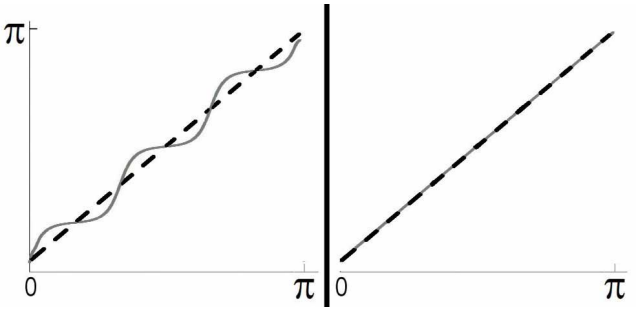

Fig. 7. The graphs represent the estimated ($\arg(I_{2,0}^{(R)})$) (full lines) as well as the accurate direction angle(dotted lines) on a upper ring in the FM-test image. Left: estimated with Gabor spectrum of 6 orientations. Right: estimated by spatial approach. fmtestEstimate.eps

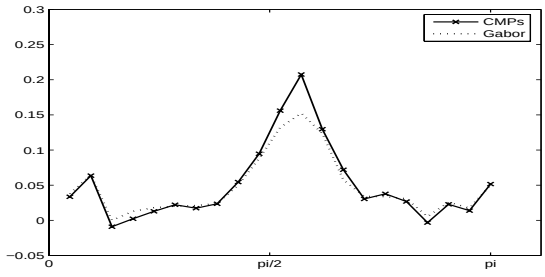

Fig. 8. The estimated power spectrum along one narrow band using Gabor filters (dotted) and CMPs (full line). Image used to estimate is the "p1" image of figure 3. p1testGab.eps